OPEN

Dapagliflozin Attenuates Heart Failure With Preserved Ejection Fraction Remodeling and Dysfunction by Elevating β-Hydroxybutyrate–activated Citrate Synthase

Xinxin Zhang, MD, PhD, Ning Wang, MM,* Peng Fu, MM,* Yanliang An, MM,* Fangfang Sun, MSC,† Chengdong Wang, MSC,† Xiao Han, PhD,‡ Yunlong Zhang, MD,‡ Xiaohong Yu, MD, PhD,* and Ying Liu, MD, PhD**

Abstract: Heart failure with preserved ejection fraction (HFpEF) is highly prevalent, accounting for 50% of all heart failure patients, and is associated with significant mortality. Sodium–glucose cotransporter subtype inhibitor (SGLT2i) is recommended in the AHA and ESC guidelines for the treatment of HFpEF, but the mechanism of SGLT2i to prevent and treat cardiac remodeling and dysfunction is currently unknown, hindering the understanding of the pathophysiology of HFpEF and the development of novel therapeutics. HFpEF model was induced by a high-fat diet (60% calories from lard) + N[w]-nitro-L-arginine methyl ester (L-NAME—0.5 g/L) (2 Hit) in male Sprague Dawley rats to effectively recapture the myriad phenotype of HFpEF. This study's results showed that administration of dapagliflozin (DAPA, SGLT2 inhibitor) significantly limited the 2-Hit–induced cardiomyocyte hypertrophy, apoptosis, inflammation, oxidative stress, and fibrosis. It also improved cardiac diastolic and systolic dysfunction in a late-stage progression of HFpEF. Mechanistically, DAPA influences energy metabolism associated with fatty acid intake and mitochondrial dysfunction in HFpEF by increasing β-hydroxybutyric acid (β-OHB) levels, directing the activation of citrate synthase, reducing acetyl coenzyme A (acetyl-CoA) pools, modulating adenosine 5′-triphosphate production, and increasing the expression of mitochondrial oxidative phosphorylation system complexes I-V. In addition, following clinical DAPA therapy, the blood levels of β-OHB and citrate synthase increased and the levels of acetyl-CoA in the blood of HFpEF patients decreased. SGLT2i plays a beneficial role in the prevention and treatment of cardiac remodeling and dysfunction in HFpEF model by attenuating cardiometabolic dysregulation.

Key Words: heart failure with preserved ejection fraction, dapagliflozin, metabolism, cardiac remodeling, β-hydroxybutyric acid

(*J Cardiovasc Pharmacol*™ 2023;82:375–388)

INTRODUCTION

Heart failure with preserved ejection fraction (HFpEF) is an increasing public health problem, accounting for 50% of all heart failure (HF) patients, and is associated with significant morbidity and mortality.[1] HFpEF has evidence of abnormal cardiac remodeling and diastolic dysfunction, with elevated natriuretic peptide levels.[2] The dynamic change in left ventricular ejection fraction (LVEF) occurs as HFpEF progresses, with a decline in LVEF at a later stage of heart failure with reduced ejection fraction (HFrEF).[1] Compared with HFrEF, specific evidence-based pharmacological or other treatments for HFpEF are limited. The lack of suitable preclinical HFpEF models to recapitulate the complexity of human HFpEF has hindered the development of new therapies.

Previous animal models of HFpEF, such as the Dal salt–sensitive rat or the spontaneously hypertensive rat, mostly emphasized hypertension, left ventricular hypertrophy, and diastolic dysfunction.[3] However, clinical patients often have hypertension and obesity/metabolic dysfunction. Emerging evidence points that mitochondrial dysfunction

Received for publication March 17, 2023; accepted August 7, 2023.

From the *Department of Cardiology, Institute of Cardiovascular Diseases; †Department of Nuclear Medicine, The First Affiliated Hospital of Dalian Medical University, Dalian, Liaoning Province, China; and ‡Department of Emergency Medicine, Beijing Key Laboratory of Cardiopulmonary Cerebral Resuscitation, Beijing Chaoyang Hospital, Capital Medical University, Beijing, China.

Supported by the National Natural Science Foundation of China (No. U1908209 and No. 81700385), Project of Liaoning Provincial Department of Education (No. LJKZ0852), and Liaoning Natural Science Foundation (No. 2022-MS-336).

The authors report no conflicts of interest.

Supplemental digital content is available for this article. Direct URL citations appear in the printed text and are provided in the HTML and PDF versions of this article on the journal's Web site (www.jcvp.org).

Y. Zhang conceived the project. Preparation of materials, data collection, and analysis were performed by X. Zhang, N. Wang, P. Fu, Y. An, F. Sun, C. Wang, and X. Han. X. Zhang and Y. Zhang wrote the manuscript, which was revised by X. Yu and Y. Liu. All authors read and approved the final manuscript.

X. Zhang and N. Wang contribute equally to this article and are considered cofirst authors.

Any material other than available from commercial sources described in this article can be obtained from the authors upon written request.

Correspondence: Ying Liu, MD, PhD or Xiaohong Yu, MD, PhD, Department of Cardiology, Institute of Cardiovascular Diseases, The First Affiliated Hospital of Dalian Medical University, 193 United Road, Dalian, Liaoning Province, 116021, China (e-mail: yingliu.med@gmail.com or yuxiaohong0707@163.com) or Yunlong Zhang, MD, Department of Emergency Medicine, Beijing Key Laboratory of Cardiopulmonary Cerebral Resuscitation, Beijing Chaoyang Hospital, Capital Medical University, Beijing, 100020, China (e-mail: zyldy111@vip.163.com).

triggered by adenosine 5′-triphosphate (ATP) energy deficiency and substrate utilization disorders is implicated in hypertension and obesity/metabolic dysfunction.[4] Meanwhile, recent studies pointing to lipotoxic accumulation (lipotoxicity) is a hallmark of metabolic alterations in cardiovascular disease.[5]

Dapagliflozin (DAPA) is a selective inhibitor of SGLT2 and is used clinically due to its inhibition of glucose reabsorption in the kidney.[6] Recent clinical trials have revealed exciting results, with DAPA significantly reducing the risk of cardiovascular death and HF events.[7] However, the mechanisms of sodium–glucose cotransporter subtype inhibitor (SGLT2i) prevention and treatment of HFpEF cardiac remodeling are currently unknown.[1] Because SGLT2i is valuable in treating cardiometabolic HFpEF phenotypes, this research hypothesized that it exerts beneficial effects by restoring HFpEF metabolic disorders. SGLT2i may improve myocardial energetics by increasing ketogenesis.[8] Ketone bodies, including β-OHB, acetoacetate, and acetone, are mainly produced in the liver of mammals.[9] Recent studies have shown that an increased abundance of β-OHB activates citrate synthase (CS), the center of mitochondrial redox processes.[10,11] However, whether DAPA exerts a beneficial effect on HFpEF and HFrEF by activating the CS has not been investigated.

This study applied a high-fat diet (HFD + L-NAME rat model with typical aspects of the cardiometabolic HFpEF phenotype that can optimally simulate HFpEF comorbidities compared with previous HFpEF models, which were termed the "2-Hit" strategy. Therefore, targeting metabolism may provide a novel approach to preventing diastolic cardiac dysfunction and structural remodeling in patients with HFpEF. This model is particularly relevant for exploring novel therapeutic interventions of the metabolic drug SGLT2i against the cardiometabolic system of HFpEF.

METHODS

Animals and Treatment

Male Sprague Dawley (SD) rats aged 2 months and weighing 240–280 g were conditioned in a room at 24–25°C with a light/dark cycle of 12 hours. A series of 6-week experiments was conducted to induce HFpEF in rats and verify the protective effect of DAPA on HFpEF. SD rats were divided into 4 groups based on their body weight. (1) control, (2) DAPA (10 mg/kg by oral gavage once daily), (3) HFD (60% calories from lard) + L-NAME (0.5 g/L in drinking water), and (4) HFD + L-NAME + DAPA for 6 weeks (n = 6).

Subsequently, the rats were kept in a 12-week trial, under the continuous effect of a "2-Hit," to test the effect of DAPA on established HFpEF progression. Six-week SD and HFD + L-NAME rats were first assessed by echocardiography (baseline) to ensure that HFD + L-NAME rats had been induced with HFpEF. After 6 weeks, SD rats were then divided by body weight into (1) control and (2) DAPA. After 6 weeks, HFpEF rats were randomly divided by body weight into (3) HFD + L-NAME and (4) HFD + L-NAME + DAPA (n = 6) and continued for an additional 6 weeks.

The study and experimental procedures were approved and performed following the review board of the Animal Care and Use Committee of Dalian Medical University (AEE1-2016-045) and conformed to the Guide for the Care and Use of Laboratory Animals (National Institutes of Health).

Blood Pressure Measurements

Rat peripheral arterial blood pressure in the tail artery was measured weekly at baseline for 2 months using a noninvasive tail-cuff system (BP-2010A; Softtron Inc., Tokyo, Japan). The tail artery was dilated using a preheated 37°C plate.[12]

Echocardiographic Assessment

Animals were anesthetized with 1.5%–2.0% doses of isoflurane (n = 6 per group). An experienced technician evaluated the cardiac function by echocardiography using Vevo 1100 High-Resolution Imaging System (Visual Sonics Inc). Parameters of left ventricular (LV) internal dimensions at end diastole and end systole (LVIDs), left ventricular anterior wall (LVAW), and left ventricular posterior wall at end systole and end diastole. The percentage of ejection fraction or shortening fraction was calculated for all rats.[12] Pulsed-wave Doppler images of mitral inflow obtained from an apical 4-chamber view were used to detect the transmitral E/A ratio, an index of LV diastolic function.[12,13]

PET/CT Imaging

Glucose and fatty acid (FA) metabolisms in the hearts of rats (n = 3 per group) were assessed by positron emission tomography (PET) using [18F]-2-fluoro-2-deoxy-D-glucose (FDG) and [18F]-6-thia-heptadecanoic acid (FTHA), which reflected the rates of glucose uptake and β-oxidation of free FA in the heart, respectively.[14] Scans were obtained with a Super Nova SNPC-103 microPET/CT scanner (Pingseng Healthcare Inc). Static PET/CT images were acquired 40 minutes after injection of [18F]-FDG (180–220 MBq) and [18F]-FTHA (free FA for myocardial PET imaging, 180–250 MBq). Images were reconstructed using Pingseng Avatar software (version 1.4.0). The acquired data were reconstructed using the Fourier-rebinned algorithm in 6 time frames (2*300 seconds, 2*600 seconds, 2*1800 seconds) and the 3-dimensional ordered-subsets expectation maximum algorithm (3D-OSEM). The heart was visualized on the short, horizontal, and vertical long axes. At a maximum local tracer activity of 41%, the region of interest was defined as LV myocardium using a contour threshold, and the standard uptake values were recorded.[15,16]

Histological Analysis

Heart tissues from each group were fixed in 4% paraformaldehyde, embedded in paraffin, and divided into 5-μm-thick sections. Sections were analyzed for histopathology using hematoxylin and eosin (H&E, Servicebio, Wuhan, China), Masson's trichrome (Vector Laboratories, Burlingame, CA), and Rhodamine-labeled wheat germ agglutinin (Vector Laboratories, Burlingame, CA) following standard procedures.[17] Sections were stained by immunohistochemistry with α-smooth muscle actin (α-

SMA, Abcam, Cambridge, MA) and Mac-2 antibody (Santa Cruz, Dallas, TX).

Frozen heart specimens were cut into 5-μm-thick sections and incubated with 10 mmol/L dihydroethidium (DHE) for DHE staining. This procedure was done for 30 minutes in a light-proof, humidified chamber at 37°C. Photographs were taken with a Nikon microscope (Nikon, Tokyo, Japan).[18] The images were analyzed using Image-Pro Plus 3.0 software. Apoptosis was detected using an in situ cell death assay kit (Roche, Basel, Switzerland) according to the protocol described.[19] Heart sections were stained using the TUNEL kit, whereby cardiac myocytes and nuclei were stained with anti-α-actin and anti-DAPI antibodies, respectively (Sigma-Aldrich, Dorset, United Kingdom). Heart sections were then imaged in 6–8 random fields of view, and the proportion of tunnel-positive nuclei was calculated, as described previously.[19]

Western Blotting Analysis

Protein extracts were obtained from frozen heart tissue using RIPA lysis buffer and quantified using a BCA assay (Thermo Fisher, Carlsbad, CA). Equal amounts (40–60 μg) of protein were separated by 8%–10% sodium dodecyl sulfate polyacrylamide gel electrophoresis. These were transferred to polyvinylidene difluoride membranes . These were blocked with 5% nonfat-dried milk in TBST for 1 hour at ambient temperature and blotted with the appropriate primary antibody overnight for 12 hours at 4°C. Densitometric analysis of all blots was performed using Image J Software (NIH) and normalized to GAPDH expression levels. Blots are cut horizontally into 2, 3, or 4 strips, detecting different proteins (such as Complex III, IV and V, and GAPDH) of different molecular weights in parallel. For phosphorylated forms of proteins, the blot is stripped with a reprocessing stripping buffer, and the total forms of the protein is detected by reprofiling. Under certain conditions, samples were run on parallel gels and were probed separately. Equal loading was controlled for all blots, and 1 representative loading control was depicted, in main figures. The antibodies used in this study are shown in **Supplemental Digital Content 1** (see **Table**, http://links.lww.com/JCVP/A983).

Citrate Synthase, Acetyl-coenzyme A, β-OHB, and ATP Content Measurements

CS activity was measured in heart and blood samples under the conditions shown by a CS activity assay kit from Sigma (MAK193). Diluted samples, reduced glutathione (GSH) standards, and positive controls were added to a 96-well plate to determine CS activity using the coupled enzyme reaction. It was followed by a reaction mixture containing a mixture of CS developer and CS substrate. The specific absorbance at 412 nm was measured every 5 minutes for 1 hour. CS activity was expressed as a percentage.

Heart and blood tissue proteins were precipitated with perchloric acid. The supernatant was neutralized after centrifugation (10,000 × *g*) by adding potassium bicarbonate. It was done until the sample pH was 6–8, and the precipitate was removed by centrifugation. Cell lysates were harvested, and acetyl-CoA levels were measured using an acetyl-CoA assay kit (Sigma-Aldrich, MAK039).

The β-OHB levels in frozen heart tissue (5–10 mg, n = 5 per group) and blood samples were measured using the β-Hydroxybutyrate Colorimetric Assay Kit (Cayman no. 700190). ATP levels in heart tissue (10 mg, n = 5 per group) were measured using ab83355 (Abcam, Cambridge, MA).

Quantitative Real-time PCR (RT-qPCR)

RNA was extracted from the LV tissue of the heart using TRIzol (Invitrogen, Carlsbad, CA), and 1 μg of messenger RNA (mRNA) was reverse-transcribed to complementary DNA using the Bio-Rad iCycler IQ system.[17] The qPCR was performed following standard procedures, with gene-specific primers for ANF and collagen I. Transcript levels were standardized to GAPDH.

Study Patients

This study considered all HF patients in an age-matched and sex-matched healthy population as a control group in a single-center clinical cohort study from January to August 2022. Patients with HFpEF and HFrEF were diagnosed based on the 2021 ESC guidelines.[2] Blood samples were collected from 15 patients with HFpEF treated with DAPA, 15 patients with HFpEF without DAPA, 15 patients with HFrEF treated with DAPA, and 15 control subjects. Plasma β-OHB levels were measured by ELISA kit (Cayman no. 700190) according to the instructions. The Ethics Committee of the First Hospital of the Dalian Medical University (No. LCKY2016-31) approved this study, which conformed to the principles outlined in the Declaration of Helsinki. Each patient signed written informed consent.

Data and Statistical Analysis

The results are expressed as means ± SEM. Comparisons between the groups were made using a two-sample Student's *t* test or nonparametric Mann–Whitney *U* test. Comparisons between more than 3 groups were made using 2-way analysis of variance. For experiments set up with >1 variable, repeated-measures 2-way analysis of variance with Sidak's multiple comparisons was used. All statistical analyses were performed using GraphPad Prism 8.0 software. A *P* value of less than 0.05 was considered a significant difference.

RESULTS

β-OHB Level and CS Activity are Decreased in 2-Hit–Treated Blood and Heart

To address the causal role of β-OHB in HFpEF development, first, we compared the circulating β-OHB concentration in healthy mice (0 weeks) and 3-, 6-, 12-week 2-Hit–treated mice. The levels of β-OHB in the myocardium and serum of mice decreased in a time-dependent manner with the extension of 2-Hit (Figs. 1A–D), indicating that the decrease of β-OHB is a potential cause for the development of HFpEF.

Immunoblotting further confirmed a time-dependent decrease in CS protein levels in 2-Hit–treated hearts

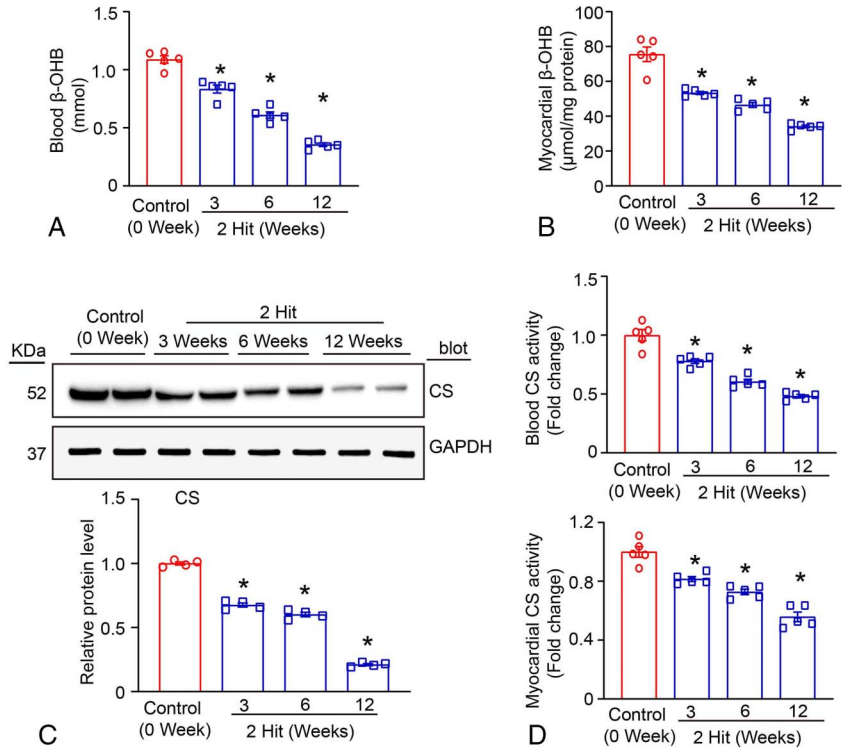

FIGURE 1. β-OHB level and CS activity are decreased in 2-Hit–treated blood and heart. (A) The blood β-OHB level in the rats (n = 5). B, The β-OHB level in hearts (n = 5). C, Immunoblotting analysis of protein levels of CS. D, The CS activity in hearts and blood (n = 5). Data are expressed as means ± SEM, and n represents number of animals, $*P < 0.05$ versus control; $\#P < 0.05$ versus 2-Hit; ns, $P > 0.05$ versus control or 2-Hit.

(Fig. 1C). Similarly, CS activity levels in the myocardium and serum of mice decreased in a time-dependent manner with the extension of 2-Hit (Fig. 1D).

DAPA Attenuated Hypertension and Improved Cardiac Dysfunction with 2-Hit Strategy HFpEF Model

Patients with HFpEF often have hypertension and obesity/metabolic dysfunction, so mechanistic imbalances in systemic inflammation and nitric oxide (NO) levels are critical to the disease development.[20] The overlap of metabolic stress (obesity/metabolic syndrome) and mechanical stress (hypertension) caused by NO dysregulation is the main pathophysiological mechanism of HFpEF.[21] This research fed 2-month-old rats an HFD + L-NAME for 6 weeks to exacerbate hypertension, systemic inflammation, and metabolic dysfunction, which was called the "2-Hit" strategy to incorporate these risk factors into 1 model (Fig. 2A).

Fasting plasma glucose levels were higher in 2-Hit rats than in control rats, and blood pressure increased over time (Figs. 2B–C). 2-Hit treatment did not alter the LVEF and fractional shortening (FS) but decreased the transmitral E/A ratio compared with control rats. The trend reflected the characteristics of diastolic dysfunction in HFpEF (Fig. 2D). In addition, the dimensions of the LVAW at end diastole were higher in the 2-Hit group compared with the control group, without a significant difference in LVID (Table 1). The SD rats treated with 2-Hit for 6 weeks recapitulated the typical pathological phenotype of HFpEF.

This study examined the pathological changes in the 2-Hit model at 6 weeks to determine the cardiopreventive effect of DAPA on HFpEF. There are indications that long-term SGLT2i leads to left ventricular reverse-remodeling secondary to reduced preload and afterload.[22] This study observed that DAPA-treated 2-Hit rats showed a significant decrease in blood pressure but remained in the hypertensive range and showed improved diastolic function (Figs. 2B–C). Furthermore, an increased E/A ratio was observed, but no significant differences were seen in LVEF, FS, and LVID (Fig. 2D). Meanwhile, DAPA treatment also resulted in lower LVAW dimensions at end diastole than in the 2-Hit group (Table 1). These results suggested that DAPA treatment attenuated hypertension and improved myocardial dysfunction in the 2-Hit group.

DAPA Alleviated HFpEF Cardiac Hypertrophy, Inflammation, Fibrosis, and Oxidative Stress

The 6-week-old 2-Hit rats resulted in pathological cardiac hypertrophy, hypertension, and compensatory cardiac hyperfunction. These were accompanied by increased fibrosis, oxidative stress, and inflammation. Relative to the control group, 2-Hit for 6 weeks in SD rats significantly accelerated myocardial hypertrophy, as shown by higher ratios of heart weight normalized to body weight (HW/BW) and heart weight normalized to tibia length (HW/TL), cardiac myocyte size, and the mRNA level of ANF. However, reversal of the above indicators was observed after the administration of DAPA; DAPA prevented 2-Hit–induced cardiac hypertrophy significantly (Figs. 3A–B). In addition, DAPA substantially inhibited severe, perivascular, interstitial fibrosis in 2-Hit hearts and α-SMA-positive myofibroblasts. It also reduced profibrosis (collagen I) mRNA expression level in 2-Hit rats

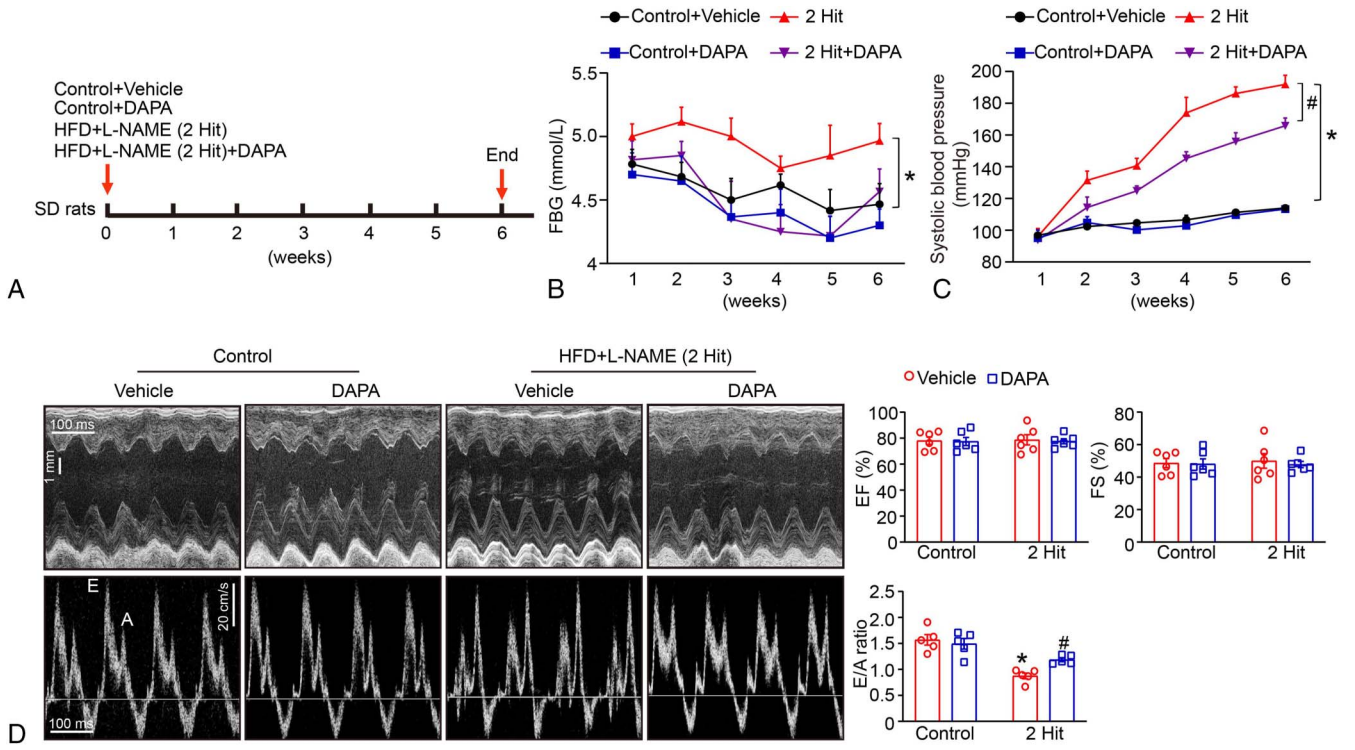

FIGURE 2. Administration of DAPA attenuated hypertension and improved cardiac dysfunction with 2-Hit strategy HFpEF in rats. (A), A schematic representation of the 2-Hit strategy. B, FBG levels (n = 6). C, SBP was measured every week by tail-cuff method (n = 6). D, M-mode echocardiography of LV chamber, and measurements of EF%, FS% and transmitral E/A ratio (n = 6). Data are expressed as means ± SEM and analyzed using repeated-measures 2-way analysis of variance and Sidak's multiple comparisons test (B–C), and n represents number of animals, $*P < 0.05$ versus control; $\#P < 0.05$ versus 2-Hit; ns, $P > 0.05$ versus control or 2-Hit. EF%, ejection fraction; FBG, fasting blood glucose; FS%, fractional shortening; SBP, systolic blood pressure.

(Figs. 3C–D). In addition, the 2-Hit model group was compared to determine whether DAPA inhibited inflammatory response and oxidative stress. This research discovered that DAPA inhibited the infiltration of inflammatory cells and Mac-2+ macrophages (Fig. 3E). DHE staining showed that DAPA treatment reduced superoxide production levels in the 2-Hit myocardium (Fig. 3F). Furthermore, 2-Hit highly upregulated ERK, NOX1/2, and P65 phosphorylation levels and TGF-β1 protein levels in hearts, whereas DAPA intervention downregulated these protein levels (Fig. 3G). It was concluded that DAPA had a significant protective effect on 2-Hit–induced HFpEF.

TABLE 1. Cardiac Echocardiographic Parameters of the 6-wk Experimental Rats

Characteristics	CTRL	DAPA	HFD + L-NAME	HFD + L-NAME + DAPA
LVEF	78.05 ± 7.151	77.46 ± 7.483	78.73 ± 9.597	77.61 ± 4.730
FS	48.61 ± 6.878	48.12 ± 7.664	49.95 ± 10.95	47.78 ± 4.716
E/A	1.467 ± 0.3213	1.462 ± 0.2180	0.8629 ± 0.1159*	1.141 ± 0.1334†
LVAW; d	1.730 ± 0.1485	1.753 ± 0.1981	2.113 ± 0.3045*	1.972 ± 0.3216
LVAW; s	2.891 ± 0.4560	3.038 ± 0.4021	3.345 ± 0.5668	3.226 ± 0.3797
LVID; d	7.428 ± 8.340	7.371 ± 0.4612	7.206 ± 0.7400	7.285 ± 1.418
LVID; s	3.843 ± 0.7581	3.848 ± 0.7612	3.607 ± 0.8934	3.811 ± 0.8741
LVPW; d	2.148 ± 0.2288	2.402 ± 0.3476	2.362 ± 0.8012	2.247 ± 0.4781
LVPW; s	3.238 ± 0.3450	3.336 ± 0.4825	3.857 ± 1.102	3.618 ± 0.5304

$*P < 0.05$ versus control.
$†P < 0.05$ versus HFD + L-NAME.
LVPW, left ventricular posterior wall.

DAPA Activated 5′-AMP–activated Protein Kinase and Improved Energy Metabolism by Inhibiting Myocardial FA Uptake in HFpEF

This study measured the uptake of myocardial glucose and FA (reflecting the rate of oxidation of FFA) at the 6 weeks using PET-CT (containing [18F]-FDG or [18F]-FTHA) to examine whether DAPA improves energy metabolism in HFpEF myocardium. DAPA treatment reduced FDG uptake compared with control, but no statistical differences were observed (Fig. 4A). Meanwhile, at 6 weeks, 2-Hit–induced HFpEF showed a 1.67-fold increase in FTHA uptake compared with the control group. DAPA treatment normalized FTHA uptake (Fig. 4b). The TUNEL assays indicated that the percentage of TUNEL-positive cells were significantly higher in 2-Hit hearts than in the control group, and these effects were markedly reduced in DAPA-treated hearts (Fig. 4C).

AMPK plays a key role in regulating glucose and FA metabolism, mitochondrial function, and cellular apoptosis in HF.[23] 2-Hit hearts showed a significant reduction in AMPK phosphorylation expression. These changes were significantly restored in the DAPA-treated hearts (Fig. 4D). In addition, mitochondria are the main producers of ATP in cardiomyocytes. ATP production was significantly lower in the 2-Hit hearts than in the control group. Myocardial ATP production was significantly improved by DAPA treatment, associated with improved mitochondrial dynamics (Fig. 4E). Overall, these results suggested that DAPA protects HFpEF hearts by inhibiting FA uptake.

DAPA Rescued the HFpEF Phenotype by Increasing β-OHB Levels and Activating CS in Rats

We found that β-OHB levels in the 2-Hit model were consistent with HFpEF patients exhibiting lower levels. With reprogramming of substrate preferences, the heart can adapt to changes in the metabolic and hormonal environment in response to stress stimuli.[24] This research observed an increase in β-OHB in DAPA-treated HFpEF myocardium associated with an increase in circulating β-OHB. In addition, BDH1 (β-OHB dehydrogenase 1), an enzyme that catalyzes the first step of β-OHB catabolism in mitochondria, immunoblotting confirmed the downregulation of BDH1 expression in DAPA-treated 2-Hit hearts. Acetyl-CoA was the end product of glycolysis, FA oxidation, and ketone body β-oxidation. This research found that DAPA treatment reduced cardiac and blood acetyl-CoA accumulation in the 2-Hit heart. It was suggested that the use of ketones as fuel in HFpEF myocardium was decreased by DAPA treatment (Figs. 5A–D, see **Figure**, **Supplemental Digital Content 1a**, http://links.lww.com/JCVP/A982).

CS controlled the flux of acetyl-CoA into the tricarboxylic acid cycle, a key regulator of the maintenance of the acetyl-CoA pool. Previous studies have demonstrated that β-OHB attenuates protein deacetylation by activating CS.[11] Moreover, CS has a protective role in angiotensin II–induced atrial fibrillation, and increased expression of CS may be a potential therapeutic option for treating atrial fibrillation.[25] This research detected a decrease in CS expression by immunoblotting in the 2-Hit model at 6 weeks, whereas DAPA increased CS expression. Meanwhile, CS activity in HFpEF myocardium and blood increased after DAPA treatment. The mitochondrial inner membrane protein complex (complexes I-V) played a key role in ATP production. Therefore, the expression of complex I-V, including NDUFB8, SDHB, UQCRC2, MTCO2, and ATP5A in the ventricles, was examined (Figs. 5E–G). It was found that the reduction in complex I-V protein levels in 2-Hit rats was significantly reversed in DAPA-treated rats. Therefore, these results suggested that increased expression of CS upregulated complex I-V expression.

DAPA Inhibited the Progression of Established HFpEF Cardiac Structural and Functional Disorders

This study tested whether DAPA could affect the progression of established HFpEF. Rats with significant HFpEF features after 6 weeks of 2-Hit were randomly divided into 2 groups: 1 group received 2-Hit along with DAPA (10 mg/kg) for an additional 6 weeks and another group continued to receive 2-Hit for 6 weeks only (Fig. 6A). Compared with the 2-Hit group, DAPA treatment decreased fasting plasma glucose levels (Fig. 6B). In addition, a gradual decrease in elevated blood pressure was observed in the DAPA-treated 2-Hit rats (Fig. 6C). Continuous 2-Hit caused progressive systolic dysfunction and further deterioration of diastolic function (decrease of LVEF, FS, and E/A ratio), appearing as HFrEF features. DAPA-treated 2-Hit rats established that HFpEF significantly reversed cardiac systolic and diastolic dysfunction (increased LVEF, FS, and E/A ratio). In control rats, there were no significant differences in these parameters in the DAPA-treated group (Fig. 6D and see **Table**, **Supplemental Digital Content 2**, http://links.lww.com/JCVP/A984).

DAPA significantly reversed established HFpEF myocardial hypertrophy, as demonstrated by decreased HW/BW and HW/TL ratios, cardiac myocyte size, and the mRNA level of ANF (Figs. 5E–F). As well as, the 2-Hit group showed elevated levels of severe perivascular, interstitial fibrosis, and fibrosis markers (α-SMA and collagen I), whereas these expressions were suppressed in the DAPA-treated rats (Figs. 6G–H). DAPA-treated rats significantly reversed the increase in Mac-2–positive macrophages and superoxide production. In control rats, there were no significant differences in these parameters in the DAPA-treated groups (Figs. 6I–J).

DAPA Improved Energy Metabolism by Inhibiting Myocardial FA Uptake and Energy Pathway Activation in Response to Established HFpEF Progression

Similar changes in FDG uptake were observed at 12 weeks; DAPA treatment reduced FDG uptake compared with control (Fig. 7A). In addition, DAPA treatment normalized established HFpEF progression FTHA uptake in 12 weeks (Fig. 7B).

Similarly, DAPA-treated rats significantly reversed the increase in apoptosis compared with the 2-Hit group (Fig. 6C).

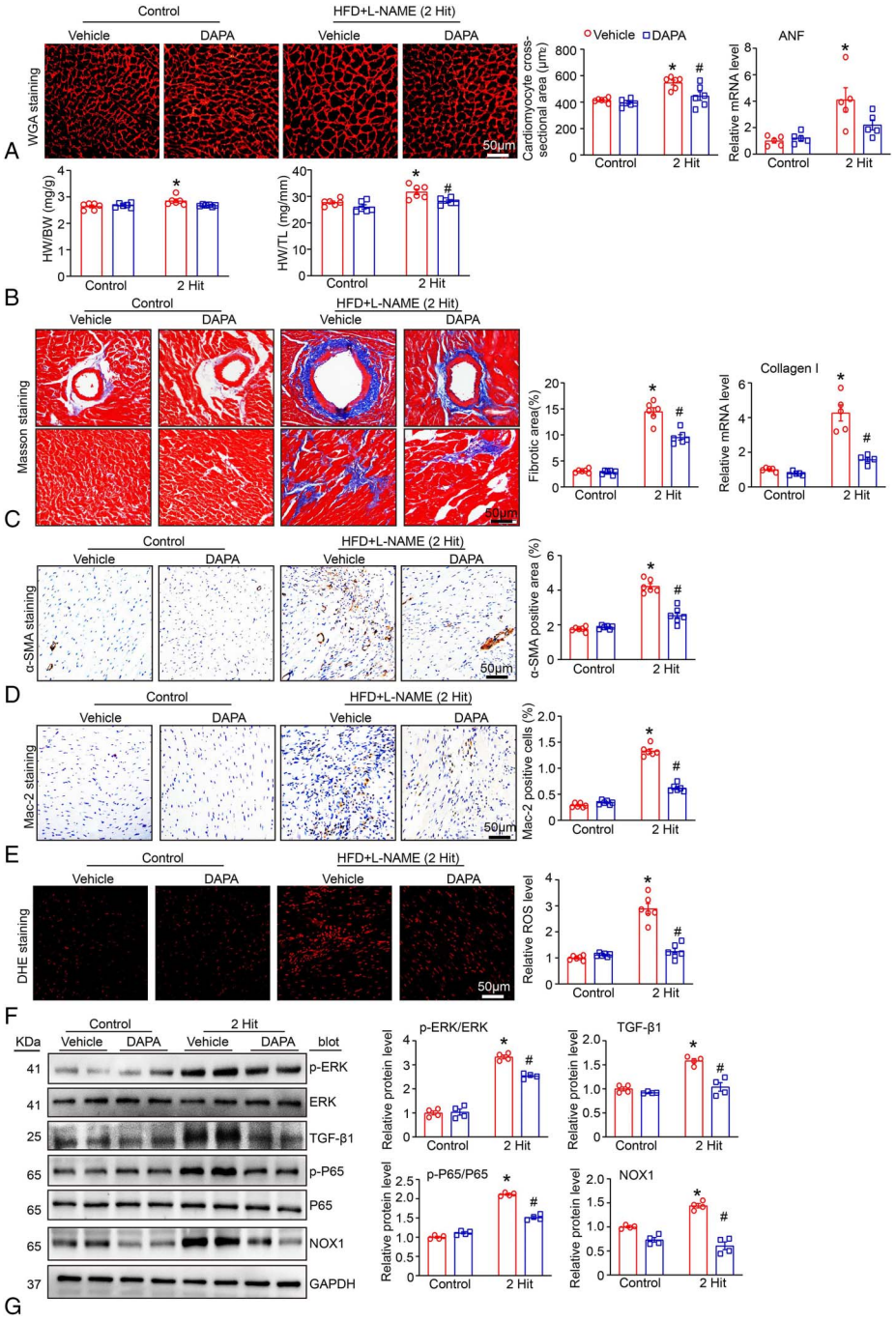

FIGURE 3. DAPA alleviated HFpEF cardiac hypertrophy, inflammation, fibrosis, and oxidative stress. A, TRITC-labeled WGA staining of heart sections (left), and quantification of cross-sectional area of myocytes (200 cells counted per heart, right, n = 6), qPCR analysis of the mRNA levels of ANF in the heart (n = 5). B, The heart weight/body weight, heart weight/TL ratios (n = 6). C, Masson's trichrome staining of heart sections (left), and quantification of myocardial interstitial and perivascular collagen deposition (right, n = 6). D, Immunohistochemical staining of cardiac myofibroblasts with anti-α-SMA antibody (left), and quantification of α-SMA–positive cells (right, n = 6). E, Representative images of immunohistochemical staining of macrophages with anti-Mac-2 antibody (left), and quantification of Mac-2–positive area (right, n = 6). F, DHE staining of heart sections (left), quantification of DHE fluorescence intensity (right, n = 6). Scale bar: 50 μm. G, Representative immunoblots of p-ERK, ERK, TGF-β1, p-P65, P65, NOX1 in heart tissues from each group (left). Quantification of the relative protein levels by densitometry (right, n = 4). Data are expressed as means ± SEM, and n represents number of animals, $*P < 0.05$ versus control; $\#P < 0.05$ versus 2-Hit; ns, $P > 0.05$ versus control or 2-Hit.

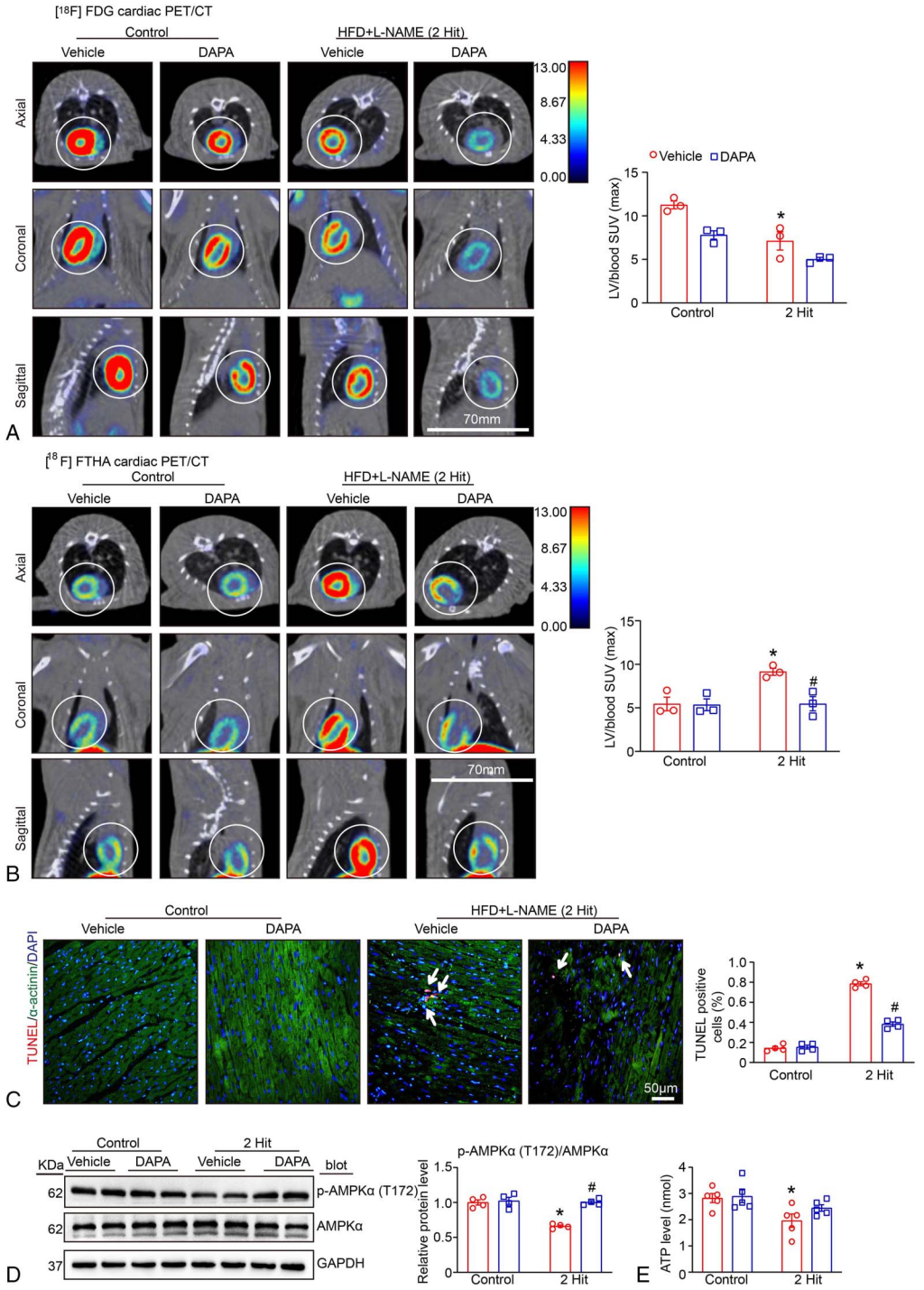

FIGURE 4. Administration of DAPA-activated 5′-AMP–activated protein kinase (AMPK) and improved energy metabolism by inhibiting myocardial FA uptake in HFpEF. A, Representative PET images of axial (top), coronal (middle), and sagittal (bottom) cardiac sections with [18F]-FDG in rats and quantification of the maximum LV SUV (right, n = 3), showing myocardial glucose uptake. B, Representative PET images: Axial (top), coronal (middle), and sagittal (bottom) cardiac sections with [18F]-FTHA in rats and quantification of the maximum LV SUV (right, n = 3), showing myocardial FA uptake. C, Representative images of TUNEL (red), α-actinin (green), and DAPI (blue) staining of the myocardial sections (left), and quantification of the TUNEL-positive nuclei (right, n = 4). Scale bar: 5 mm or 20 μm. D, Immunoblotting analysis of the protein levels of p-AMKP (T172), GAPDH as an internal control (left), and the quantification of the relative protein levels (right, n = 4). E, Measurement of ATP contents (n = 5). Data are expressed as means ± SEM, and n represents number of animals, $*P < 0.05$ versus control; $\#P < 0.05$ versus 2-Hit; ns, $P > 0.05$ versus control or 2-Hit. SUV, standard uptake values.

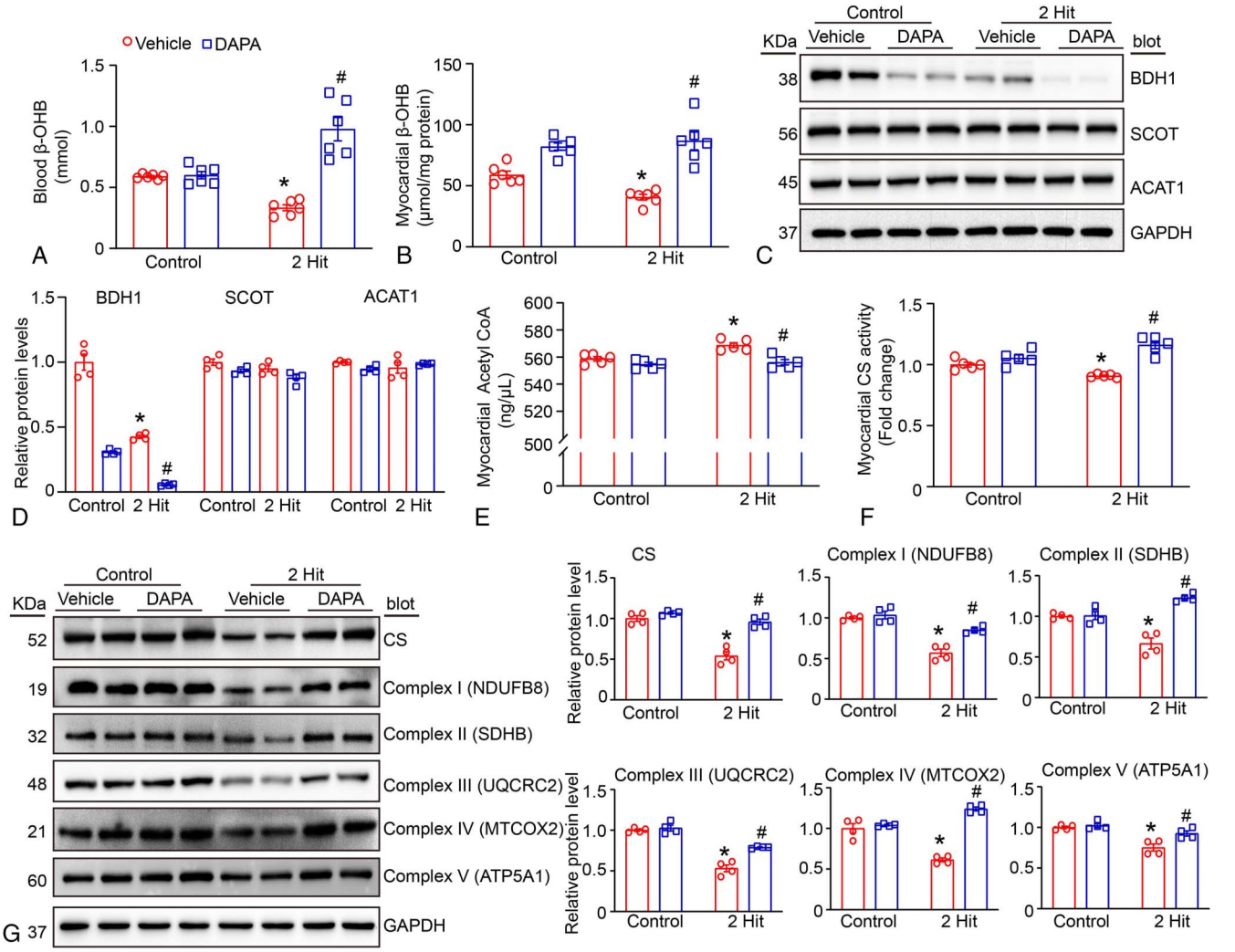

FIGURE 5. Administration of DAPA rescued the HFpEF phenotype by increasing β-OHB levels and activating CS in rats (A), The blood β-OHB level in the rats (n = 6). B, The β-OHB level in hearts (n = 6). C, Representative immunoblots of BDH1, SCOT, and ACAT1 in heart tissues from each group. D, Quantification of the relative BDH1, SCOT, ACAT1 protein levels by densitometry (n = 4). E, The acetyl-CoA level in hearts (n = 5). F, The CS activity in hearts (n = 5). G, Immunoblotting analysis of protein levels of CS, mitochondrial complex I (NDUFB8), complex II (SDHB), complex III (UQCRC2), complex IV (MTCO2), and complex V (ATP5A) (left), and quantification of the relative protein level (n = 4). Data are expressed as means ± SEM, and n represents number of animals, $*P < 0.05$ versus control; $\#P < 0.05$ versus 2-Hit; ns, $P > 0.05$ versus control or 2-Hit.

DAPA treatment increased cardiac AMPK phosphorylation expression and increased ATP production in 2-Hit hearts. β-OHB, acetyl-CoA, and CS levels had similar trends to HFpEF in established HFpEF progression (Figs. 7D,I, see **Figure**, **Supplemental Digital Content 1b**, http://links.lww.com/JCVP/A982). These results suggested that DAPA can reverse established HFpEF cardiac structural and functional disorders by modulating metabolic abnormalities.

DAPA Treatment in HFpEF and HFrEF Patients Elevated Blood β-OHB and CS Levels and Reduced Acetyl-CoA Levels

This research analyzed blood β-OHB, CS, and acetyl-CoA levels and other cardiovascular risk factors to examine whether β-OHB, CS, and acetyl-CoA are important in human HFpEF. The tests were conducted in HFpEF patients with DAPA treatment (n = 15), HFpEF patients without DAPA treatment (n = 15), HFrEF patients with DAPA treatment (n = 15), and normal subjects (n = 15) (Table 2). Consistent with the in vivo results, HFpEF and HFrEF patients showed increased blood β-OHB and CS levels and decreased acetyl-CoA levels after DAPA treatment (Figs. 8A–C). Overall, these results suggest that improved metabolic abnormalities by DAPA may be a mechanism in the pathogenesis and progression of HFpEF.

DISCUSSION

This study described a 2-Hit rat model that replicated key hemodynamic features in patients with HFpEF. This model was used to identify the interaction of CS in metabolic

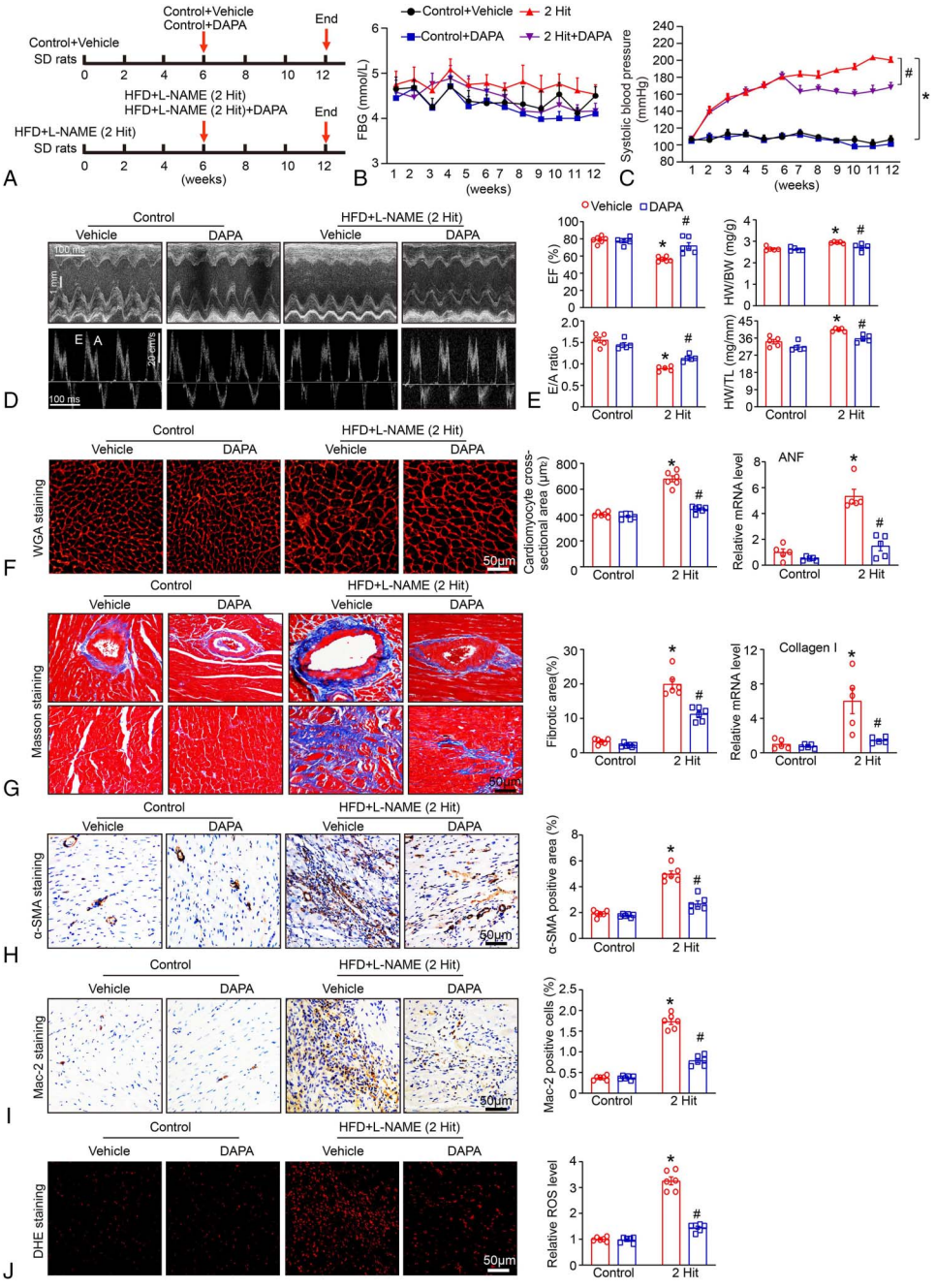

FIGURE 6. Administration of DAPA inhibited the progression of established HFpEF cardiac structural and functional disorders (A), SD and 2-Hit rats at 6 weeks were administered with DAPA or vehicle control for additional 6 weeks. The following experiments were performed up to the end of 12 w. B, FBG levels (n = 6). C, SBP was measured every week by tail-cuff method (n = 6). D, M-mode echocardiography of left ventricular chamber, and measurement of EF%, FS% transmitral E/A ratio (n = 6). E, The heart mass/body mass, heart mass/TL ratios (n = 6). F, TRITC-labeled WGA staining of heart sections (left), and quantification of cross-sectional area of myocytes (200 cells counted per heart, right, n = 6), qPCR analysis of the mRNA levels of ANF in the heart (n = 5). G, Masson's trichrome staining of heart sections (left), and quantification of myocardial interstitial and perivascular collagen deposition (right, n = 6), qPCR analysis of the mRNA levels of collagen I in the heart (n = 5). H, Immunohistochemical staining of cardiac myofibroblasts with anti-α-SMA antibody (left), and quantification of α-SMA–positive cells (right, n = 6). I, Representative images of immunohistochemical staining of macrophages with anti-Mac-2 antibody (left), and quantification of Mac-2–positive area (right, n = 6). J, DHE staining of heart sections (left) and quantification of DHE fluorescence intensity (right, n = 6). Scale bar: 50 μm. Data are expressed as means ± SEM, and n represents number of animals, $*P < 0.05$ versus control; $\#P < 0.05$ versus 2-Hit; ns, $P > 0.05$ versus control or 2-Hit. EF%, ejection fraction; FBG, fasting blood glucose; FS%, fractional shortening; SBP, systolic blood pressure.

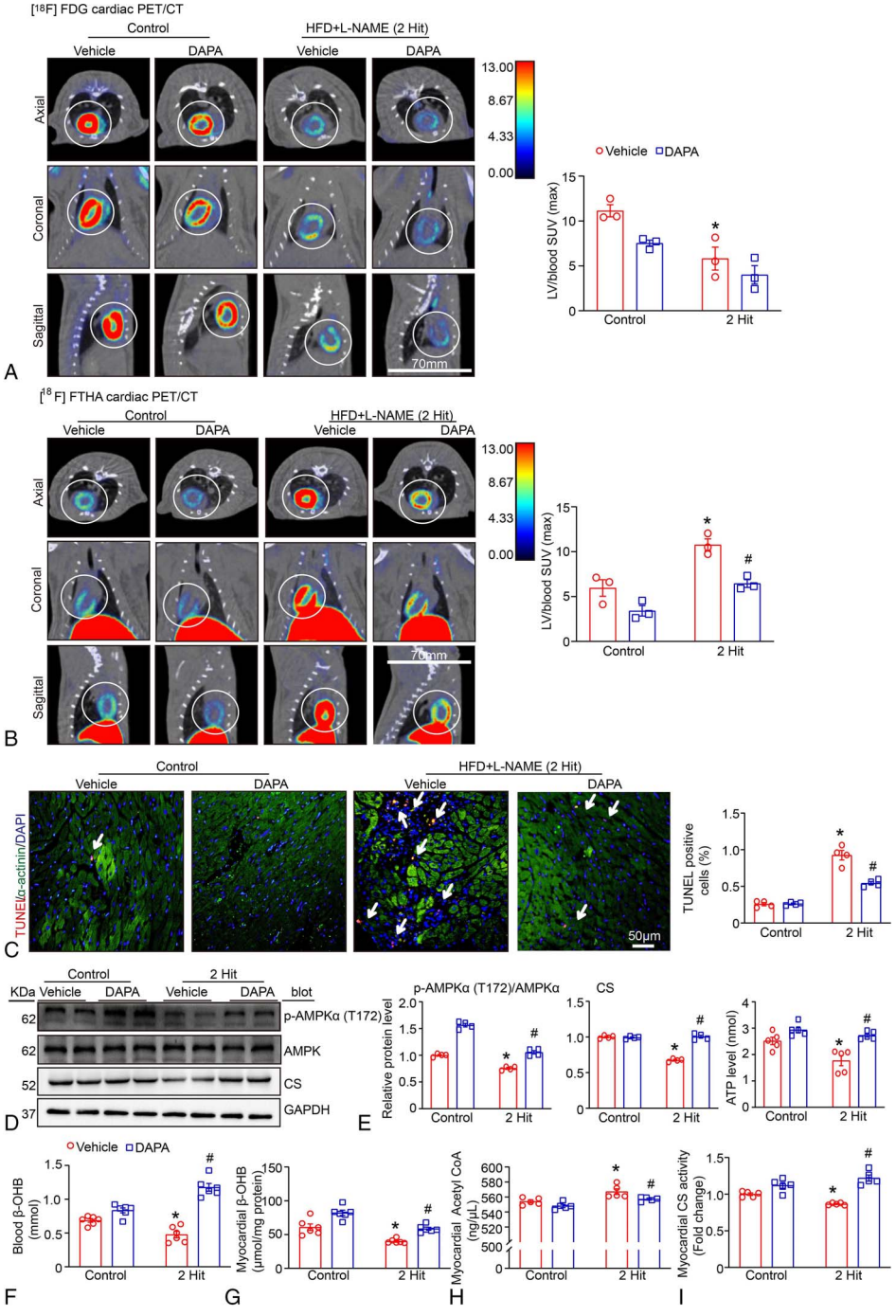

FIGURE 7. Administration of DAPA improved energy metabolism by inhibiting myocardial FA uptake and energy pathway activation in response to established HFpEF progression. A, Representative PET images of axial (top), coronal (middle), and sagittal (bottom) cardiac sections with [18F]-FDG in rats and quantification of the maximum LV SUV (right, n = 3) showing myocardial glucose uptake. B, Representative PET images: Axial (top), coronal (middle), and sagittal (bottom) cardiac sections with [18F]-FTHA in rats and quantification of the maximum LV SUV (right, n = 3) showing myocardial FA uptake. C, Representative images of TUNEL (red), α-actinin (green), and DAPI (blue) staining of the myocardial sections (left) and quantification of the TUNEL-positive nuclei (right, n = 4). Scale bar: 5 mm or 20 μm. D, Immunoblotting analysis of the protein levels of p-AMKP (T172) and CS, GAPDH as an internal control (left), and the quantification of the relative protein levels (right, n = 4). E, Measurement of ATP contents (n = 5). F, The blood β-OHB level in the rats (n = 6). G, The β-OHB level in hearts (n = 6). H, The acetyl-CoA level in hearts (n = 5). I, The CS activity in hearts (n = 5). Data are expressed as means ± SEM, and n represents number of animals, $*P < 0.05$ versus control; $\#P < 0.05$ versus 2-Hit; ns, $P > 0.05$ versus control or 2-Hit. SUV, standard uptake values.

TABLE 2. Baseline Demographics and Clinical Characteristics of Patients

Characteristics	Control	HFpEF	HFpEF + DAPA	HFrEF + DAPA
Number of patients	15	15	15	15
Age (yr), mean (SD)	63.47 ± 4.307	67.87 ± 9.583	65.87 ± 13.32	65.73 ± 8.705
Male	7 (46.67%)	8 (53.33%)	10 (66.67%)	10 (66.67%)
Blood pressure (mm Hg), mean (SD)	126.9 ± 10.10	132.5 ± 25.10	126.5 ± 18.70	104.5 ± 15.14*
Systolic				
Diastolic	78.47 ± 8.340	73.33 ± 15.62	72.47 ± 10.43	71.00 ± 12.99
LVEF (%)	59.00 ± 3.381	54.67 ± 3.792	55.67 ± 3.677	26.93 ± 6.017*
Laboratory values, median (IQR)				
White blood cell	5.957 ± 1.449	5.471 ± 1.597	6.409 ± 1.344	5.960 ± 1.300
×10^9/L				
Creatinine, umol/L	66.40 ± 20.01	127.1 ± 81.28	125.6 ± 53.48	102.9 ± 43.74
Alanine	20.73 ± 12.08	15.00 ± 5.682	20.93 ± 9.750	21.87 ± 15.08
U/L				
Aspartic acid	20.00 ± 8.089	19.00 ± 5.555	24.60 ± 9.627	23.40 ± 8.584
U/L				
Triglyceride, mmol/L	1.054 ± 0.6726	1.483 ± 0.6113	1.165 ± 0.4407	1.128 ± 0.3997
Cholesterol, mmol/L	3.754 ± 0.5480	4.067 ± 1.176	3.861 ± 1.213	4.423 ± 1.170
Glucose, mmol/L	5.349 ± 0.6510	5.579 ± 1.379	5.208 ± 0.8474	5.381 ± 1.151

*$P < 0.05$ versus control.

disturbances in HFpEF, a driver of HFpEF pathogenesis. Furthermore, it was validated in the established HFpEF progression. CS, a central regulator of mitochondrial redox in energy metabolism, was significantly downregulated in the 2-Hit hearts. DAPA decreased the acetyl-CoA pool by increasing β-OHB levels, activating CS, increasing the expression of the mitochondrial oxidative phosphorylation system complex I-V and ATP production, and resulting in improved mitochondrial function. It also inhibits FA uptake to reduce myocardial hypertrophy, fibrosis, inflammation, oxidative stress, and apoptosis, preventing systolic dysfunction from occurring in the late progression of HFpEF (Fig. 8D).

Due to the comorbidities of HFpEF, there is a significant overlap between its molecular and cellular abnormalities. It is observed in diabetes and obesity, including metabolic defects in fuel utilization and efficiency, inflammatory responses, lipotoxicity, pathological growth of cardiomyocytes, and cytoprotective signaling loss.[3] Meanwhile, the dynamics of LVEF trajectories are of increasing interest, and late progression of HFpEF disease is often combined with abnormal systolic function on the basis of diastolic dysfunction.[1] Previous studies have shown that in a nondiabetic mouse model of transverse aortic constriction, which initially manifests as HFpEF but evolves to HFrEF at a late stage, although 2 weeks of treatment with empagliflozin did not improve structural remodeling (LV volumes, mass), it significantly slowed the progressive decline in cardiac function compared with controls, but the transverse aortic constriction model, as a model of hypertrophic cardiomyopathy, does not effectively recapture the abnormal metabolic features of HFpEF.[26] This study showed that 2-Hit significantly promoted myocardial hypertrophy and dysfunction with increased fibrosis, apoptosis, oxidative stress, and inflammation. The administration of DAPA was effective in preventing and treating 2-Hit–induced cardiac hypertrophy, fibrosis, apoptosis, oxidative stress, and inflammation.

CS, a central regulator of mitochondria-related signaling pathways, was significantly reduced in the 2-Hit heart, but reactive oxygen species levels increased, leading to inflammation, fibrosis, and HFpEF development. As the first rate-limiting enzyme in the tricarboxylic acid cycle, CS plays a decisive role in regulating the production of ATP in mitochondrial.[27] Radlinger et al showed that mitochondrial mass, as estimated by CS activity, was significantly elevated in SGLT2i-treated mice, but it is questionable whether SGLT2i directly affects cardiac metabolism through CS activity.[28] SGLT2i stimulates lipolysis by reducing insulin levels, promoting ketones' hepatic production.[29] Therefore, SGLT2i induced mild ketosis in diabetic and nondiabetic subjects. Ketone bodies, including β-OHB, acetoacetate, and acetone, are mainly produced in the liver of mammals.[9] This finding was consistent with the results of this article. It has been proposed that increased ketone body oxidation in the failing heart may increase acetyl-CoA, increasing the hyperacetylation of mitochondrial proteins and exacerbating mitochondrial respiratory dysfunction.[30] Mitochondria play a key role in the heart's energetics (ATP production) that maintain normal electrical and mechanical function. The 5 oxidative phosphorylation system complexes necessary for ATP synthesis by mitochondria are NADH dehydrogenase (complex I), succinate dehydrogenase (complex II), cytochrome c reductase (complex III), cytochrome c oxidase (complex IV), and ATP synthase (complex V).[31] In this study, we found that elevated β-OHB levels induced by DAPA preventive intervention and treatment were effective in improving mitochondrial function. The results showed that DAPA inhibited the expression of BDH1 and that the expression levels of other enzymes of ketone body metabolism (SCOT, ACAT1) were not changed, which is consistent with the study by Deng et al,[11]

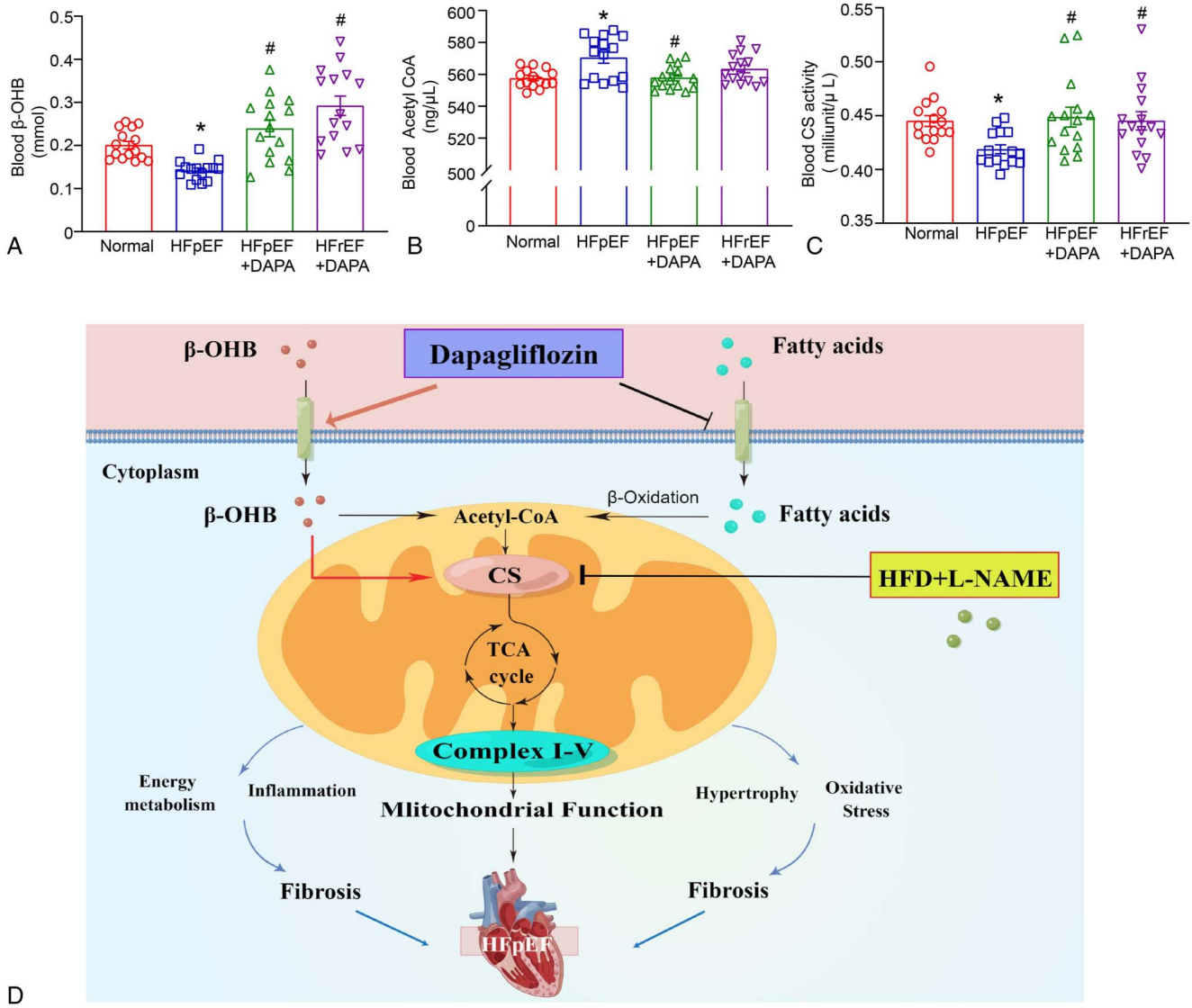

FIGURE 8. DAPA attenuated a working model of HFpEF remodeling and dysfunction by elevating β-hydroxybutyrate (β-OHB)–activated CS, 2-Hit initiated hypertension, inflammation, oxidative stress, and induced cardiac hypertrophy and fibrosis. These lead to cardiac remodeling in HFpEF. Subsequently, the elevation of β-hydroxybutyrate by DAPA attenuated these effects. A, The β-OHB level in blood samples of normal controls (n = 15), HFpEF patients (n = 15), HFpEF patients with DAPA (n = 15), and HFrEF patients with DAPA (n = 15). B, The acetyl-CoA level in blood samples of normal controls (n = 15), HFpEF patients (n = 15), HFpEF patients with DAPA (n = 15), and HFrEF patients with DAPA (n = 15). C, The CS activity in blood samples of normal controls (n = 15), HFpEF patients (n = 15), HFpEF patients with DAPA (n = 15), and HFrEF patients with DAPA (n = 15). D, A schematic illustration of DAPA attenuates HFpEF remodeling and dysfunction by elevating β-hydroxybutyrate-activated CS. Data are expressed as means ± SEM, and n represents number of patients, *$P < 0.05$ versus control; #$P < 0.05$ versus HFpEF patients; ns, $P > 0.05$ versus control or HFpEF patients.

suggesting that β-OHB does not provide substrate for oxidation but increases ATP production without impairing mitochondrial respiratory function by activating CS and reducing the accumulation of the acetyl-CoA pool.

The perturbations produced by ATP directly alter the systolic and diastolic functions and lead to HF.[32] In patients with HF, derangements in substrate utilization and intermediate metabolism, energy deficiency, and oxidative stress underlie diastolic and systolic dysfunction and disease progression.[4] However, few metabolic interventions prevent or treat these diseases.[33] Compared with a normal healthy heart, a failing heart shows an energy deficit and produces less ATP, possibly due to the altered availability of cardiac energy substrates and impaired mitochondrial oxidative capacity.[33] Meanwhile, metabolic inflexibility and the toxic intermediate accumulation, rather than unbalanced substrate utilization, may adversely affect cardiac function.[4] AMPK is a key energy sensor that critically regulates glucose uptake, glycolysis, and FA oxidation.[34] Our results showed that DAPA

treatment resulted in AMPK activation and significantly improved ATP production in 2-Hit hearts.

Metabolic disorders underlie a variety of cardiovascular disease states. Changes in systemic and cardiac metabolism precede the development of HF.[35] Impaired adaptation of energy metabolism during cardiac hypertrophy exacerbates pathological hypertrophy and increases cardiomyocyte death.

Glucose and FA uptake were measured using [^{18}F] FDG and FTHA in PET, respectively. Furthermore, DAPA inhibited 2-Hit–induced FA uptake, improving mitochondrial dynamics. These findings suggested that DAPA ameliorates 2-Hit–induced cardiomyocyte remodeling and dysfunction by improving myocardial energy metabolism. Certainly, we need to clarify that the 2-Hit model was used in this study, and energy metabolism associated with FA intake leading to mitochondrial dysfunction plays a main role in the induction of HFpEF. The current beneficial results of DAPA may largely depend on the phenotype of HFpEF. By contrast, the effect of blood triglyceride levels may be lower in the hypertension-dominated TAC model, and the beneficial effect of DAPA may be lower than in the 2-Hit model.

Consistent with the in vivo trial, this study measured human blood β-OHB levels and found that plasma β-OHB concentrations were significantly higher in HFpEF patients treated with DAPA than in HFpEF patients without DAPA and controls. Furthermore, decreased acetyl-CoA levels and significantly higher CS activity were observed. This suggests that clinical DAPA treatment may influence HFpEF onset and late progression by improving myocardial metabolic abnormalities, which would provide more potential possibilities for future HFpEF treatment.

REFERENCES

1. Heidenreich PA, Bozkurt B, Aguilar D, et al. 2022 AHA/ACC/HFSA guideline for the management of heart failure: executive summary: a report of the American College of Cardiology/American Heart Association Joint Committee on Clinical Practice Guidelines. *Circulation*. 2022. 145, e876-e894.
2. McDonagh TA, Metra M, Adamo M, et al. 2021 ESC Guidelines for the diagnosis and treatment of acute and chronic heart failure. *Eur Heart J*. 2021. 42, 3599–3726.
3. Mishra S, Kass DA. Cellular and molecular pathobiology of heart failure with preserved ejection fraction. *Nat Rev Cardiol*. 2021;18:400–423.
4. Bertero E, Maack C. Metabolic remodelling in heart failure. *Nat Rev Cardiol*. 2018;15:457–470.
5. Schiattarella GG, Rodolico D, Hill JA Metabolic inflammation in heart failure with preserved ejection fraction. *Cardiovasc Res*. 2021;117:423–434.
6. de Leeuw AE, de Boer RA. Sodium-glucose cotransporter 2 inhibition: cardioprotection by treating diabetes—a translational viewpoint explaining its potential salutary effects. *Eur Heart J Cardiovasc Pharmacother*. 2016;2:244–255.
7. Packer M, Anker SD, Butler J, et al. Cardiovascular and renal outcomes with empagliflozin in heart failure. *N Engl J Med*. 2020;383:1413–1424.
8. Ferrannini E, Mark M, Mayoux E. CV protection in the EMPA-REG OUTCOME trial: a "Thrifty Substrate" hypothesis. *Diabetes Care*. 2016; 39:1108–1114.
9. Puchalska P, Crawford PA. Multi-dimensional roles of ketone bodies in fuel metabolism, signaling, and therapeutics. *Cell Metab*. 2017;25:262–284.
10. Horton JL, Davidson MT, Kurishima C, et al. The failing heart utilizes 3-hydroxybutyrate as a metabolic stress defense. *JCI Insight*. 2019;4: e124079.
11. Deng Y, Xie M, Li Q, et al. Targeting mitochondria-inflammation circuit by beta-hydroxybutyrate mitigates HFpEF. *Circ Res*. 2021;128:232–245.
12. Zhang YL, Geng C, Yang J, et al. Chronic inhibition of chemokine receptor CXCR2 attenuates cardiac remodeling and dysfunction in spontaneously hypertensive rats. *Biochim Biophys Acta Mol Basis Dis*. 2019; 1865:165551.
13. Zhang YL, Li PB, Han X, et al. Blockage of fibronectin 1 ameliorates myocardial ischemia/reperfusion injury in association with activation of AMP-LKB1-AMPK signaling pathway. *Oxid Med Cell Longev*. 2022; 2022:1–13.
14. Hernandez AM, Huber JS, Murphy ST, et al. Longitudinal evaluation of left ventricular substrate metabolism, perfusion, and dysfunction in the spontaneously hypertensive rat model of hypertrophy using small-animal PET/CT imaging. *J Nucl Med*. 2013;54:1938–1945.
15. Drozd K, Ahmadi A, Deng Y, et al. Effects of an endothelin receptor antagonist, Macitentan, on right ventricular substrate utilization and function in a sugen 5416/hypoxia rat model of severe pulmonary arterial hypertension. *J Nucl Cardiol*. 2017;24:1979–1989.
16. Blanc-Durand P, Jegou S, Kanoun S, et al. Fully automatic segmentation of diffuse large B cell lymphoma lesions on 3D FDG-PET/CT for total metabolic tumour volume prediction using a convolutional neural network. *Eur J Nucl Med Mol Imaging*. 2021;48:1362–1370.
17. Chen C, Zou LX, Lin QY, et al. Resveratrol as a new inhibitor of immunoproteasome prevents PTEN degradation and attenuates cardiac hypertrophy after pressure overload. *Redox Biol*. 2019;20:390–401.
18. Wu YX, Han X, Chen C, et al. Time series gene expression profiling and temporal regulatory pathway analysis of angiotensin II induced atrial fibrillation in mice. *Front Physiol*. 2019;10:597.
19. Xie X, Bi HL, Lai S, et al. The immunoproteasome catalytic β5i subunit regulates cardiac hypertrophy by targeting the autophagy protein ATG5 for degradation. *Sci Adv*. 2019;5:eaau0495.
20. Chirinos JA, Zamani P. The nitrate-nitrite-NO pathway and its implications for heart failure and preserved ejection fraction. *Curr Heart Fail Rep*. 2016;13:47–59.
21. Schiattarella GG, Altamirano F, Tong D, et al. Nitrosative stress drives heart failure with preserved ejection fraction. *Nature*. 2019;568:351–356.
22. Verma S, Mazer CD, Yan AT, et al. Effect of empagliflozin on left ventricular mass in patients with type 2 diabetes mellitus and coronary artery disease: the EMPA-HEART CardioLink-6 randomized clinical trial. *Circulation*. 2019;140:1693–1702.
23. Koyani CN, Plastira I, Sourij H, et al. Empagliflozin protects heart from inflammation and energy depletion via AMPK activation. *Pharmacol Res*. 2020;158:104870.
24. Ritterhoff J, Tian R. Metabolism in cardiomyopathy: every substrate matters. *Cardiovasc Res*. 2017;113:411–421.
25. Teng F, Han X, Yu P, et al. Time series proteome profile analysis reveals a protective role of citrate synthase in angiotensin II-induced atrial fibrillation. *J Hypertens*. 2022;40:765–775.
26. Byrne NJ, Parajuli N, Levasseur JL, et al. Empagliflozin prevents worsening of cardiac function in an experimental model of pressure overload-induced heart failure. *JACC: Basic Transl Sci*. 2017;2:347–354.
27. de Castro Bras LE, Cates CA, DeLeon-Pennell KY, et al. Citrate synthase is a novel in vivo matrix metalloproteinase-9 substrate that regulates mitochondrial function in the postmyocardial infarction left ventricle. *Antioxid Redox Signaling*. 2014;21:1974–1985.
28. Radlinger B, Hornsteiner F, Folie S, et al. Cardioprotective effects of short-term empagliflozin treatment in db/db mice. *Sci Rep*. 2020;10:19686.
29. Bonner C, Kerr-Conte J, Gmyr V, et al. Inhibition of the glucose transporter SGLT2 with dapagliflozin in pancreatic alpha cells triggers glucagon secretion. *Nat Med*. 2015;21:512–517.
30. Horton JL, Martin OJ, Lai L, et al. Mitochondrial protein hyperacetylation in the failing heart. *JCI Insight*. 2016;2:e84897.
31. Signes A, Fernandez-Vizarra E. Assembly of mammalian oxidative phosphorylation complexes I-V and supercomplexes. *Essays Biochem*. 2018; 62:255–270.
32. Doenst T, Nguyen TD, Abel ED. Cardiac metabolism in heart failure: implications beyond ATP production. *Circ Res*. 2013;113:709–724.
33. Yurista SR, Chong CR, Badimon JJ, et al. Therapeutic potential of ketone bodies for patients with cardiovascular disease: JACC State-of-the-Art review. *J Am Coll Cardiol*. 2021;77:1660–1669.
34. Herzig S, Shaw RJ. AMPK: guardian of metabolism and mitochondrial homeostasis. *Nat Rev Mol Cell Biol*. 2018;19:121–135.
35. Liew CW, Xu S, Wang X, et al. Multiphasic regulation of systemic and peripheral organ metabolic responses to cardiac hypertrophy. *Circ Heart Fail*. 2017;10:e003864.